Journal of Applied Physics

Optimization of connection architectures and mass distributions for metamaterials with multiple resonators

Cite as: J. Appl. Phys. **129**, 165101 (2021); https://doi.org/10.1063/5.0047391
Submitted: 12 February 2021 . Accepted: 12 April 2021 . Published Online: 23 April 2021

Wenming Wei, Shuwei Ren, Dimitrios Chronopoulos, and Han Meng

Journal of Applied Physics ARTICLE scitation.org/journal/jap

Optimization of connection architectures and mass distributions for metamaterials with multiple resonators

Cite as: J. Appl. Phys. **129**, 165101 (2021); doi: 10.1063/5.0047391
Submitted: 12 February 2021 · Accepted: 12 April 2021 ·
Published Online: 23 April 2021

Wenming Wei,[1] Shuwei Ren,[2] Dimitrios Chronopoulos,[3,4] and Han Meng[5,a)]

AFFILIATIONS

[1]State Key Laboratory for Manufacturing Systems Engineering, Xi'an Jiaotong University, Xi'an, ShaanXi 710049, China
[2]School of Marine Science and Technology, Northwestern Polytechnical University, Xi'an, ShaanXi 710072, China
[3]Institute for Aerospace Technology & The Composites Group, University of Nottingham, NG8 1BB, United Kingdom
[4]Department of Mechanical Engineering & Division of Mecha(tro)nic System Dynamics (LMSD), KU Leuven, Ghent Technology Campus, 9000 Ghent, Belgium
[5]Department of Mechanical and Construction Engineering, Northumbria University, Newcastle, NE1 8ST, United Kingdom

[a)]**Author to whom correspondence should be addressed:** menghan1989.123@gmail.com

ABSTRACT

Metamaterials with multiple resonators have been widely investigated for the purpose of generating multiple stop bands or broadening the attenuation bandwidth. The multiple resonators could be connected end to end in a line, namely, in-series connection, or connected individually to the host structures, namely, in-parallel connection. This paper investigates the influence of the resonator connection methodology on the frequency response functions of metamaterial beams with multiple resonators and exhibits an approach for optimizing their resonator distribution over the structure. The receptance functions of metamaterial beams with various resonator connection architectures are calculated by a transfer matrix model, which is verified through finite element model results. It is demonstrated that resonator interconnection architectures have a great impact on the global dynamic properties of metamaterials. An optimization strategy is subsequently proposed to find out the optimal resonator connection architectures and mass distributions that could minimize the maximal receptance functions in targeted single and multiple frequency ranges. The objective functions within single targeted frequency ranges are solved by the adoption of the genetic algorithm method. The weighted sum method is used to gain an optimal solution for multi-frequency range optimization. The metamaterial beams with optimal resonator connection methods and mass distributions demonstrate greatly enhanced vibration attenuation at frequencies of interest compared with other beams. The work is expected to provide the necessary theoretical basis and incentive for future researchers working on the design of metamaterials with extended, tuned, and optimized stop bands.

I. INTRODUCTION

Metamaterials are artificially designed materials with unique properties that cannot be achieved by natural bulk materials. Metamaterials have attracted much attention in the past decades with original reports about them being related to electromagnetic and optical metamaterials.[1–3] Elastoacoustic metamaterials are the mechanical counterpart of electromagnetic and optical ones. Composed of base components and mechanical oscillators, elastoacoustic metamaterials possess unique properties such as negative mass and dynamic stiffness, negative bulk modulus, and spectral gaps, within which the propagation of waves is inhibited, also known as bandgaps or stop bands. Stop bands are of critical importance for vibration suppression of structures. Stop bands are mainly generated by two mechanisms, Bragg scattering and local resonance. Bragg scattering is caused by the interference of incident and reflected waves in periodic lattice structures (i.e., phononic crystals), hence start occurring

when the wavelengths are twice as long as the lattice dimensions. By contrast, local resonances are due to oscillating inclusions in the metamaterials and can take place at frequency ranges lower than that of Bragg scattering.

The first research using elastoacoustic metamaterials was put forward by Liu *et al.*;[4] they fabricated sonic crystals with periodic hard cores and soft coatings. The sonic crystal exhibited stop bands, where the lattice dimensions were two orders of magnitude smaller than the wavelengths. After that, a great number of elastoacoustic metamaterials were designed with a range of resonators. For instance, studies (e.g., Yang *et al.*,[5,8] Huang *et al.*,[6] Zhang *et al.*,[7,10] Wang *et al.*[9]) focused on metamaterials with a negative mass/density, which were composed of membranes with attached masses. Researchers also (e.g., Fang *et al.*,[11] Mahesh and Mini,[12] Casarini *et al.*,[13] Gebrekidan *et al.*,[14] Liu *et al.*,[15] Yamamoto,[16] Tang *et al.*[17]) proposed metamaterials with Helmholtz resonators, which showed negative elastic modulus. A few others (e.g., Maurya *et al.*[18] and Liang *et al.*[19]) proposed metamaterials by coiling up space to obtain double negativity.

Elastoacoustic metamaterials were initially created with a single resonator in each unit, and metamaterials with multiple resonators were subsequently developed to obtain multi-frequency stop bands and extend their bandwidths. Peng et al.,[20] Wang *et al.*,[21] Zhu et al.,[22] Pai et al.,[23] and Xiao et al.[24] investigated engineering structures containing multiple mass-spring subsystems. Huang and Sun,[25] Chen et al.,[26] and Li et al.[27–29] proposed metamaterial lattices composed of multiple resonating mass-in-mass systems. Meng *et al.*[30–33] developed and optimized beams with multiple rainbow shaped cantilever-mass resonators, while Liu *et al.*[14–16] proposed acoustic metamaterial panels incorporating an array of Helmholtz resonators with different resonance frequencies.

The resonators and host components of these metamaterials can come in different architectures as mentioned above, the multiple resonators are, however, typically linked by standard connection methods, i.e., in-parallel and in-series connections or combinations of these. With analogy to electrical circuits, in-series connected resonators are linked end to end along a single path. Typical instances of in-series connections could be seen by metamaterial rods, beams, and plates incorporating multi-stage mass-spring oscillators.[20,24,34–37] It is noted that only one of the mass-spring resonators was attached directly to the base structures, others were linked in a sequence. By contrast, resonators by in-parallel connection are connected individually to the host structures. For instance, Shuguang *et al.*,[38] Xiao *et al.*,[39] and Zhu *et al.*[22] presented metamaterial beams with arrays of oscillators in the units; each oscillator was attached to the beam and separated from others.

Although the in-parallel and in-series methods are widely adopted in the design and construction of multi-resonator metamaterials, the impact of the resonator connection architectures on vibration attenuation within the stop bands and the resulting frequency response function (FRF) has not been investigated, let alone the optimization of resonator connection methods and mass distributions. We hereby report an investigation into how the connection architectures and mass distributions of multiple resonators can affect the vibration performance of metamaterial beams. We also present an optimization scheme to search for optimal architectures that are able to maximize structural performance within specified frequency bands, given a finite amount of added mass and resonator numbers. It should be noted that different from the optimization of metamaterials in the previous literature that focused on the optimization of resonator mass distributions,[33] the optimization in the present paper aims at optimizing the resonator connection architectures as well as the mass distributions.

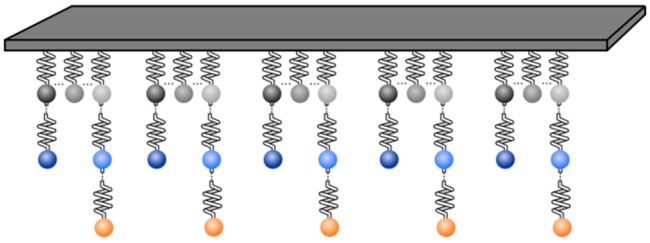

FIG. 1. Schematic diagram of a metamaterial beam with multiple resonators of different resonator connection architectures.

The present paper is structured as: metamaterial beams with various resonator connection methods are modeled by a transfer matrix method in Sec. II, which is subsequently validated by finite element (FE) models in Sec. III. Beams with different resonator architectures are compared with the analytical model in Sec. IV. The optimization methods and cases are elaborated in Sec. V.

II. ANALYTICAL MODEL

In order to perform the optimization of the metamaterial beam, an analytical model is proposed in this section to calculate the FRFs of beams with multiple resonators as shown in Fig. 1. The resonators propose different connection architectures, including single, in-series where the resonators are connected end-to-end to form a chain, and in-parallel where the resonators or resonator chains are connected individually to the panels. The transfer matrix method that has been widely used to model the wave propagation in periodic structures[40–44] is used to set up the analytical model.

Each unit cell of the beam is divided into multiple segments by the attached resonators/resonator chains as shown in Fig. 2, the displacement of each segment can be written according to the Euler Bernoulli beam theory, as

$$w_{n,j}(x) = \alpha_{n,j}e^{-ik_0(x-(x_{n-1}+p_{j-1}L_d))} + \beta_{n,j}e^{-k_0(x-(x_{n-1}+p_{j-1}L_d))} + \chi_{n,j}e^{ik_0(x-(x_{n-1}+p_{j-1}L_d))} + \varepsilon_{n,j}e^{k_0(x-(x_{n-1}+p_{j-1}L_d))}, \quad (1)$$

where $j = 1, 2, 3, \ldots, q+1$, q is the number of resonators/resonator chains attached to a unit cell of the beam, p_jL_d are the locations of resonators/resonator chains at each unit cell, L_d is the unit cell length of the beam. The flexural wavenumber value is

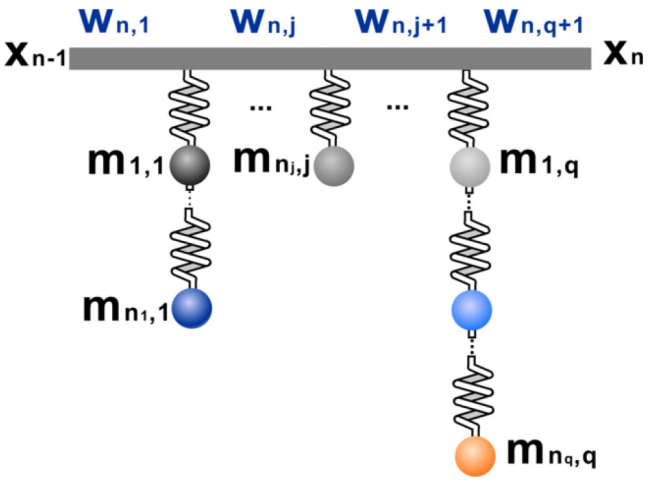

FIG. 2. A unit cell of the metamaterial beam with multiple resonators. q represents the number of in-parallel connected resonators/resonator chains in the unit cell, w_{nj} ($j = 1, 2, \ldots, q+1$) is the displacement of the jth segment of the beam, x_{n-1} and x_n are the locations of the two ends of the nth unit cell in the beam, $n_1, \ldots, n_q$ represents the numbers of in-series connected resonators in each resonator chain. m_{ij} ($j = 1, 2, \ldots, q$, $i = 1, 2, \ldots, n_j$) is the mass of the ith resonator in the jth resonator chain.

expressed as $k_0 = \left(\frac{\rho A}{EI_z}\right)^{1/4}\sqrt{\omega}$, with ρ being the density of the beam, and A and I_z being the cross-sectional area and second moment of area of the beam, respectively.

Each attached resonator/or resonator chain could be treated as exerted forces on the beam. For single resonators as shown in Fig. 3(a), the equilibrium equations of the single spring-mass system at the nth unit cell could be described by

$$m_r\ddot{z} - k(w_n - z) - c(\dot{w}_n - \dot{z}) = 0, \tag{2}$$

where z is the displacement of the mass, w_n is the displacement of the beam at the interface between the beam and resonators; k, c, and m_r are the stiffness, damping ratio, and the mass of the oscillator, respectively.

The interaction force between the host beam and the resonator is thus obtained as

$$F_a = -k(w_n - z) - c(\dot{w}_n - \dot{z}) = Q_a w_n, \tag{3}$$

where $Q_a = \frac{\omega^2 m_r(k+i\omega c)}{(-\omega^2 m_r + k + i\omega c)}$.

With regard to the in-series resonator chain as shown in Fig. 3(b), the equilibrium equations of the resonators could be described by

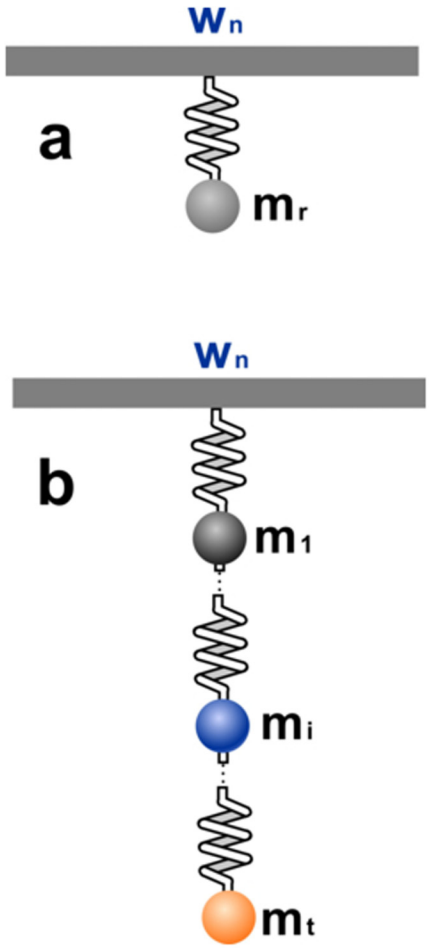

FIG. 3. Schematic diagram of (a) single resonator, (b) in-series resonator chain.

$$\begin{aligned}
&m_1\ddot{z}_1 + k_2(z_1 - z_2) + c_2(\dot{z}_1 - \dot{z}_2) - k_1(w_n - z_1) - c_1(\dot{w}_n - \dot{z}_1) = 0,\\
&m_i\ddot{z}_i + k_{i+1}(z_i - z_{i+1}) + c_{i+1}(\dot{z}_i - \dot{z}_{i+1}) - k_i(z_{i-1} - z_i) - c_i(\dot{z}_{i-1} - \dot{z}_i) = 0,\\
&m_t\ddot{z}_t - c_t(\dot{z}_{t-1} - \dot{z}_t) - k_t(z_{t-1} - z_t) = 0,
\end{aligned} \tag{4}$$

where $t = 1, 2, 3, \ldots$ is the number of in-series connected resonators in the resonator chain. Furthermore, z_i ($i = 1, 2, 3, \ldots t$) is the displacement of the ith mass, k_i, c_i, and m_i are the stiffness, damping ratio, and mass of the ith oscillator, respectively.

The interaction force between the resonator chain and the beam can be expressed as

$$F_a = -k_1(w_n - z_1) - c_1(\dot{w}_n - \dot{z}_1) = Q_a w_n, \tag{5}$$

where

$$Q_a = d_1(-1 + \boldsymbol{T}_{in}(1))w_n,\ \ d_i = k_i + j\omega c_i$$
$$\boldsymbol{T} = \begin{bmatrix} -\omega^2 m_1 + d_1 + d_2 & -d_2 & & \\ & \cdots & & \\ -d_i & -\omega^2 m_i + d_i + d_{i+1} & -d_{i+1} & \\ & \cdots & & \\ & & -d_t & -\omega^2 m_t + d_t \end{bmatrix}. \tag{6}$$
$$\boldsymbol{b} = [d_1 \quad 0 \quad \ldots \quad 0]^T,\ \ \boldsymbol{T}_{in} = \boldsymbol{T}^{-1}\boldsymbol{b}$$

According to the continuity of displacement, slope, equilibrium equations for the bending moment and shearing force at the resonator–beam interface, the displacements of the jth and $(j+1)$th segments are related as

$$\begin{aligned} w_{n,j}|_{x=x_{n-1}+p_jL_d} &= w_{n,j+1}|_{x=x_{n-1}+p_jL_d}, \\ w'_{n,j}|_{x=x_{n-1}+p_jL_d} &= w'_{n,j+1}|_{x=x_{n-1}+p_jL_d}, \\ w''_{n,j}|_{x=x_{n-1}+p_jL_d} &= w''_{n,j+1}|_{x=x_{n-1}+p_jL_d}, \\ EI_z w'''_{n,j}|_{x=x_{n-1}+p_jL_d} + F_{a,j} &= EI_z w'''_{n,j+1}|_{x=x_{n-1}+p_jL_d}, \end{aligned} \tag{7}$$

where $F_{a,j}$ $(j = 1,\ 2,\ \ldots,\ q)$ is the interaction force between the jth resonators/resonator chains and the beam calculated by Eqs. (3) and (5).

Substitution of Eq. (1) into Eq. (7) yields

$$[\alpha_{n,j+1}, \beta_{n,j+1}, \chi_{n,j+1}, \varepsilon_{n,j+1}]^T = \boldsymbol{T}_{nj}[\alpha_{n,j}, \beta_{n,j}, \chi_{n,j}, \varepsilon_{n,j}]^T, \tag{8}$$

where

$$\begin{aligned} &\boldsymbol{T}_{nj} = \boldsymbol{T}_B^{-1}\boldsymbol{T}_{fj}\boldsymbol{D}_j \\ &\boldsymbol{T}_{fj} = \begin{bmatrix} 1 & 1 & 1 & 1 \\ -ik_0 & -k_0 & ik_0 & k_0 \\ -k_0^2 & k_0^2 & -k_0^2 & k_0^2 \\ (EI_z ik_0^3 + Q_{a,j}) & (-EI_z k_0^3 + Q_{a,j}) & (-EI_z ik_0^3 + Q_{a,j}) & (EI_z k_0^3 + Q_{a,j}) \end{bmatrix}, \\ &\boldsymbol{D}_j = \mathrm{diag}(e^{-ik_0(p_j - p_{j-1})L_d}, e^{-k_0(p_j - p_{j-1})L_d}, e^{ik_0(p_j - p_{j-1})L_d}, e^{k_0(p_j - p_{j-1})L_d}), \\ &\boldsymbol{T}_B = \begin{bmatrix} 1 & 1 & 1 & 1 \\ -ik_0 & -k_0 & ik_0 & k_0 \\ -k_0^2 & k_0^2 & -k_0^2 & k_0^2 \\ EI_z ik_0^3 & -EI_z k_0^3 & -EI_z ik_0^3 & EI_z k_0^3 \end{bmatrix}. \end{aligned} \tag{9}$$

Displacement transfer matrix $\boldsymbol{T}_n$ between the nth and $(n+1)$th unit cells can hence be derived by

$$[\alpha_{n+1,1}, \beta_{n+1,1}, \chi_{n+1,1}, \varepsilon_{n+1,1}]^T = \boldsymbol{T}_n[\alpha_{n,1}, \beta_{n,1}, \chi_{n,1}, \varepsilon_{n,1}]^T, \tag{10}$$

where $\boldsymbol{T}_n = \boldsymbol{D}_{nR}\boldsymbol{T}_{nU}\boldsymbol{T}_{n(U-1)} \ldots \boldsymbol{T}_{n1}$, $\boldsymbol{D}_{nR} = \mathrm{diag}(e^{-ik_0(1-p_U)L_d}, e^{-k_0(1-p_U)L_d}, e^{ik_0(1-p_U)L_d}, e^{k_0(1-p_U)L_d})$.

Assuming that the metamaterial beam is composed of m unit cells, the beam is excited by a force F at one end and the other end is free, it is then derived that

$$\begin{aligned} EI_z w'''_{1,1}|_{x=0} &= F, \\ EI_z w''_{1,1}|_{x=0} &= 0, \\ EI_z w'''_{M,U+1}|_{x=ML_d} &= 0, \\ EI_z w''_{M,U+1}|_{x=ML_d} &= 0. \end{aligned} \tag{11}$$

The relationship between the two ends of the beam could be obtained on the basis of the transfer matrix given by Eq. (10), as

$$[\alpha_{M+1,1}, \beta_{M+1,1}, \chi_{M+1,1}, \varepsilon_{M+1,1}]^{T_S[\alpha_{1,1},\beta_{1,1},\chi_{1,1},\varepsilon_{1,1}]^T}, \tag{12}$$

where $\boldsymbol{T}_S = \boldsymbol{T}_m \boldsymbol{T}_{m-1} \boldsymbol{T}_{m-2} \cdots \boldsymbol{T}_1$.

Combing Eqs. (11) and (12) yields

$$\begin{bmatrix} \alpha_{M+1,1} \\ \beta_{M+1,1} \\ \chi_{M+1,1} \\ \varepsilon_{M+1,1} \end{bmatrix} = \boldsymbol{T}_S \boldsymbol{T}_A^{-1} \begin{bmatrix} F \\ 0 \\ 0 \\ 0 \end{bmatrix}, \tag{13}$$

where

$$\begin{aligned} \boldsymbol{T}_A &= [\boldsymbol{M}_{d1}, \boldsymbol{M}_{d2}, \boldsymbol{M}_{d3}, \boldsymbol{M}_{d4}]^{\mathrm{T}}, \\ \boldsymbol{M}_{d1} &= \begin{bmatrix} EI_z i k_0^3 & -EI_z k_0^3 & -EI_z i k_0^3 & EI_z k_0^3 \end{bmatrix}, \\ \boldsymbol{M}_{d2} &= \begin{bmatrix} -k_0^2 & k_0^2 & -k_0^2 & k_0^2 \end{bmatrix}, \\ \boldsymbol{M}_{d3} &= \begin{bmatrix} i k_0^3 & -k_0^3 & -i k_0^3 & k_0^3 \end{bmatrix} \boldsymbol{T}_s, \\ \boldsymbol{M}_{d4} &= \begin{bmatrix} -k_0^2 & k_0^2 & -k_0^2 & k_0^2 \end{bmatrix} \boldsymbol{T}_s. \end{aligned} \tag{14}$$

The receptance function of the metamaterial beam can be calculated by the above equations as

$$R_{ec} = 20 \log_{10} \left| \frac{\alpha_{M+1,l} + \beta_{M+1,l} + \chi_{M+1,l} + \varepsilon_{M+1,l}}{F} \right|. \tag{15}$$

III. VALIDATION OF THE ANALYTICAL MODEL

The analytical model is validated in this section. Receptance functions estimated by the exhibited analytical model are compared with that derived through FE calculations. The FE method has been widely used and verified by experiments to model elastoacoustic metamaterials.[34,40,45–50]

The FE models are built with the use of the solid mechanics module of Comsol Multiphysics. The metamaterial structures were treated as linear elastic materials. Unit cells of FE models of the beams with in-series and in-parallel resonators are shown in Figs. 4(a) and 4(b). The length of each beam unit is 100 mm, and the width and thickness are 20 and 2 mm, respectively. The host beam is made of aluminum with a density of 2700 kg/m^3 and a Young's modulus of 70 GPa. Each unit contains eight resonators. The masses and stiffnesses of the resonators are

$$\begin{aligned} [m_1, m_2, \ldots, m_8] &= \left[\frac{0.9}{8}, \frac{0.8}{8}, \frac{0.7}{8}, \frac{0.6}{8}, \frac{0.3}{8}, \frac{0.2}{8}, \frac{0.25}{8}, \frac{0.25}{8} \right] M_a, \\ [k_1, k_2, \ldots, k_8] &= 4\pi^2 \begin{bmatrix} 160^2 m_1, & 180^2 m_2, & 200^2 m_3, & 225^2 m_4, \\ 250^2 m_5, & 275^2 m_6, & 475^2 m_7, & 500^2 m_8 \end{bmatrix}, \end{aligned} \tag{16}$$

where M_a is the mass of the unit cell of the host beam.

The receptance functions estimated by the analytical model and FE models are compared in Figs. 5(a) and 5(b). It can be seen that the analytical results agree well with that calculated by FE models for both beams. Minor differences might be introduced by the assumptions and simplifications in the analytical model. A_p, B_p, ..., H_p and A_s, B_s, C_s are the resonance frequencies of the beams with in-parallel and in-series resonators within their bandgaps, respectively. The modal shapes of the metamaterial beams with in-parallel and in-series resonators at these resonance frequencies are also solved out by the numerical models as shown in Figs. 5(c) and 5(d), respectively. It should be noted that the mesh convergence study of FE models is given out in Appendix A. It can be seen from Fig. 5(c) that, for the beam with in-parallel resonators, one resonator dominates at each resonance frequency, which means that the bandgaps of the beam with in-parallel resonators are determined by the resonance of each individual resonator. On the contrary, regarding the metamaterial beam with in-series resonators, the bandgaps are attributed to the resonances of the in-series resonator chain instead of each individual resonator as can be seen in Fig. 5(d).

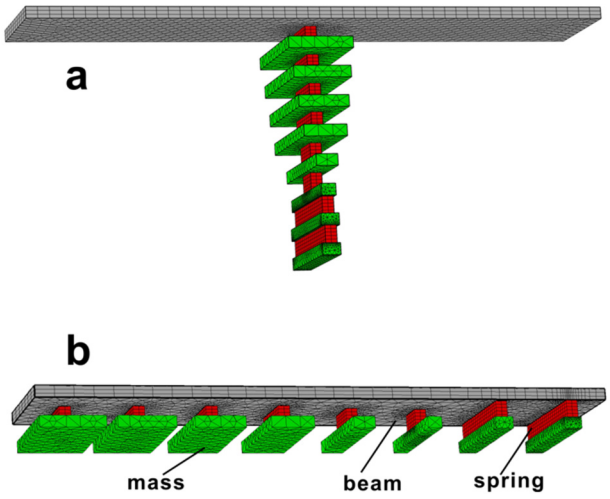

FIG. 4. Unit cells of the FE models of metamaterial beams with in-series (a) and in-parallel (b) resonators. Eight mass blocks (in green) are connected to the host aluminum beam (in gray) by springs (in red).

IV. COMPARISON OF BEAMS WITH DIFFERENT RESONATOR CONNECTION ARCHITECTURES

The FRFs of beams with single, in-parallel, and in-series resonators are discussed in this section with the use of the abovementioned analytical model. Influences of resonator mass distributions on the stop bands of the metamaterial beams are explored.

Receptance functions of the beam with single resonators are illustrated by the contour map shown in Fig. 6. The aluminum host beam contains 10 units with a height, width, and unit length of 2.5, 10, and 30 mm, respectively. The stiffness of the resonators is 500 N/m. The stop band within which the receptance functions are greatly reduced can also be seen in Fig. 6. It can be seen that, with the increase in the resonator mass, the bandwidth of the stop band

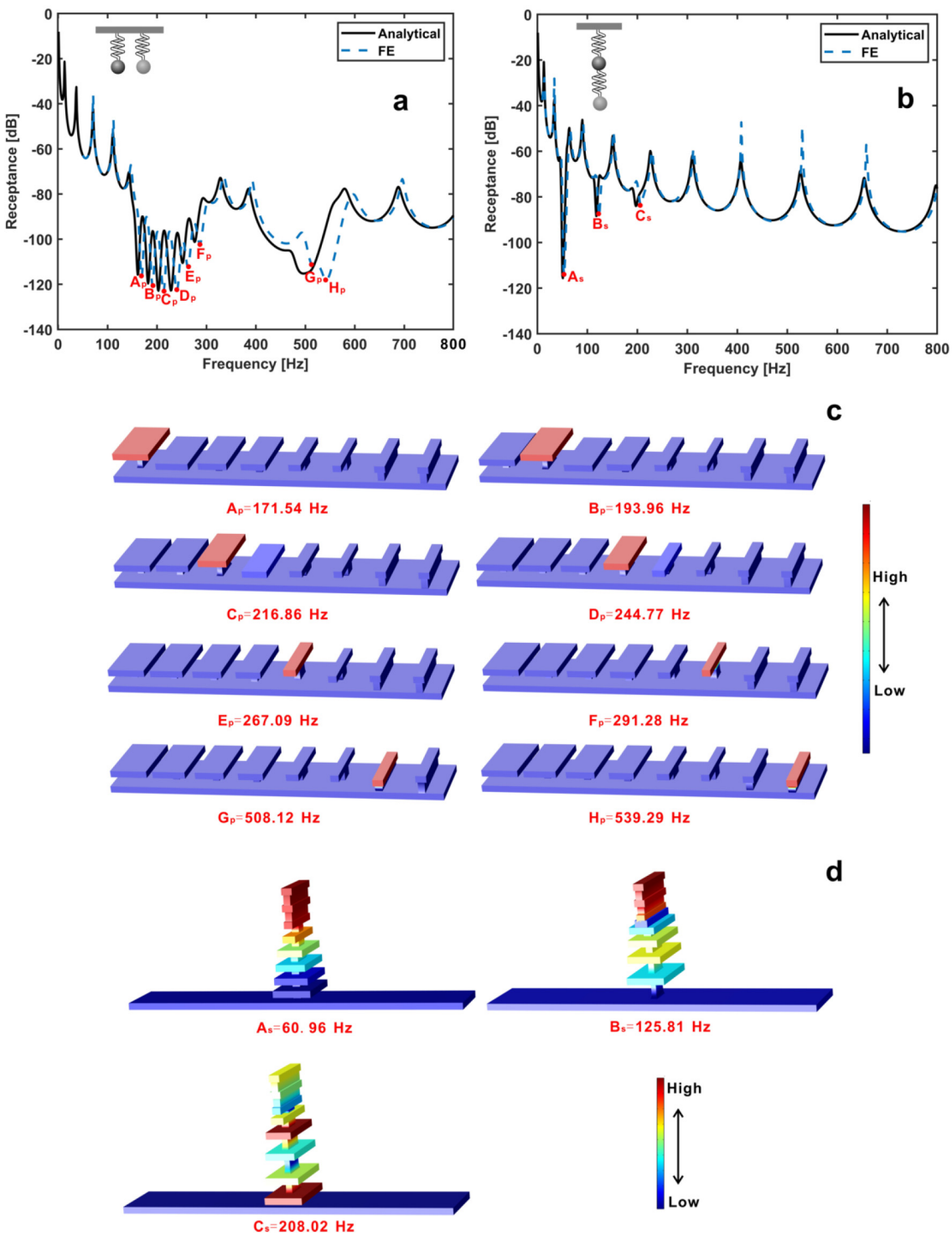

FIG. 5. Receptance function comparisons between analytical (solid line) and FE (dashed line) models of metamaterial beams with (a) in-parallel resonators and (b) in-series resonators. A_p, B_p, ..., H_p and A_s, B_s, C_s are the natural frequencies of the beams with in-parallel and in-series resonators within their bandgaps, respectively. The modal shapes of the two beams at A_p, B_p, ..., H_p and A_s, B_s, C_s are shown in (c) and (d).

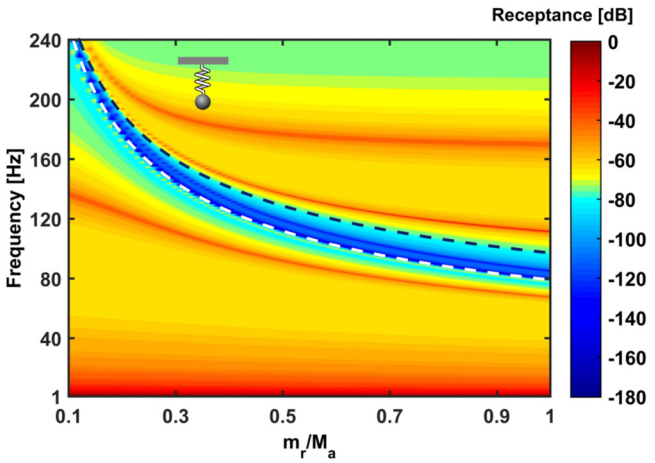

FIG. 6. Contour map of transmittance for beams with single resonators. The stop band region is marked by the white and black dashed lines. m_r and M_a are the masses of the resonator and the host beam unit, respectively.

where the receptance functions are greatly reduced increases and frequencies of the stop band decrease conversely, which is favorable for the application of metamaterials. Nonetheless, resonators with large masses could impose an excessive burden to the structures in applications. Enlarging the mass of resonators is hence not an ideal strategy to obtain broad stop bands.

Next, the FRFs of beams with in-parallel and in-series resonators are discussed. We consider beams with dual resonators in each unit for simplification. The influences of mass distributions on the receptance functions of beams with in-series and in-parallel resonators are shown in Figs. 7(a) and 7(b), respectively. The host beams have the same physical and geometric parameters as those with single resonator. The total mass of the two resonators in each unit cell are set as $0.3\,M_a$. It can be seen that, different from single resonator in each unit cell, multiple resonators lead to multiple bandgaps. The FRFs of the beams also vary dramatically with the resonator connection methods. As shown in Fig. 7(a), the in-series resonators result in two separate stop bands, the bandgap frequency of the second stop band is larger, while the bandwidth much smaller than that of the first stop band. By contrast, the in-parallel resonators generate two bandgaps that overlap when the two resonators have close masses as shown in Fig. 7(b).

V. OPTIMIZATION OF RESONATOR CONNECTION ARCHITECTURE AND MASS DISTRIBUTIONS

As mentioned above, the resonator connection architectures and mass distributions play an important role in the FRFs of metamaterial beams, hence an optimization strategy is hence developed in this section to explore the resonator connection methods and mass distributions that maximize the vibration attenuation within targeted frequency ranges.

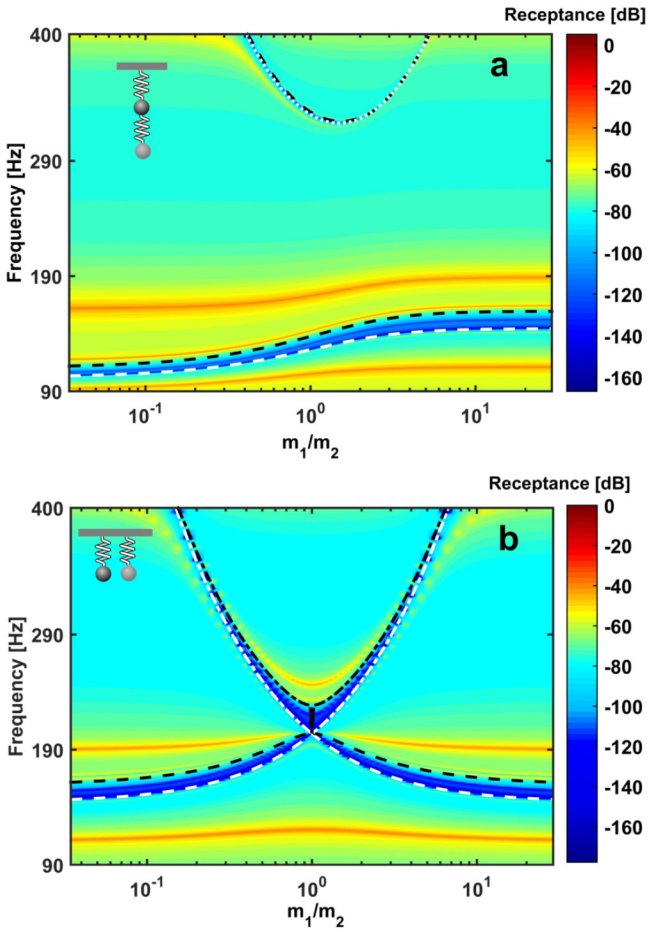

FIG. 7. Contour map of receptance values for beams with (a) in-series (b) in-parallel dual resonators. The total masses of two resonators are set as $0.3M_a$. The stop band regions are marked by the white and black dashed lines. m_1 and m_2 are the masses of the two resonators in each unit cell of the metamaterial beam.

A. Optimization objective functions

1. Single frequency range optimization

The vibration attenuation could be regarded as maximal when the maximal value of receptance functions is minimized at frequencies of interest. The objective function is thus defined as

$$\begin{aligned} \min \quad & f = \max\left[R_{ec}(q, n_1, \ldots, n_q, [m_{ij}], \boldsymbol{\Phi})\right], \\ s.t. \quad & m_{\min} \le m_{ij} \le m_{\max}, \end{aligned} \tag{17}$$

where q represents the number of in-parallel connected resonators/resonator chains in each unit cell, $n_1, \ldots, n_q$ represents the numbers of in-series connected resonators in each resonator chain, and m_{ij} $(j = 1, 2, \ldots, q,\ i = 1, 2, \ldots, n_j)$ is the mass of the ith

resonator in the jth resonator chain as shown in Fig. 2. $\boldsymbol{\Phi}$ is the targeted frequency range for optimization. The receptance functions can be predicted by Eq. (15).

2. Multi-frequency range optimization

The optimization of vibration attenuation within multiple frequency ranges can be performed by

$$\begin{aligned} \min \quad & f = [\max(f_1),\ \max(f_2),\ \ldots] \\ & f_1 = R_{ec}(q, n_1, \ldots, n_q, [m_{ij}], \boldsymbol{\Phi}_1), \\ & f_2 = R_{ec}(q, n_1, \ldots, n_q, [m_{ij}], \boldsymbol{\Phi}_2), \ \ldots \\ s.t. \quad & m_{\min} \le m_{ij} \le m_{\max}, \end{aligned} \tag{18}$$

where $\boldsymbol{\Phi}_1$, $\boldsymbol{\Phi}_2$, ... are the multiple targeted frequency ranges. The above function is composed of multiple objective functions, no resonator connection architectures and distributions exist that can simultaneously minimize the maximal receptance functions within all frequency ranges. The constituting objective functions thus are conflicting and competing since none of the objective functions would be achieved without being prejudicial to the other objective value. A Pareto optimal solution instead of a "real" optimization solution is explored to find out a trade-off design among all involved objective functions. The weighted sum method that can combine all the multi-objective functions with weight factors is adopted to develop a new single objective function, as

$$\min \quad f = \max[\kappa_1 R_{ec}(\boldsymbol{\Phi}_1) + \kappa_2 R_{ec}(\boldsymbol{\Phi}_2) + \cdots], \tag{19}$$

where κ_1, κ_2, ... are the weight factors of the frequency ranges, whose values of weight factors could be adjusted according to requirements in applications.

B. Optimization case studies

To display the feasibility of the optimization strategy, we conduct optimization studies in this section. The host beam and stiffness of resonators are the same as that used in the last section. The total mass of the resonators in each unit cell is set less than $0.3\,M_a$, and a maximal of 10 resonators are attached to each unit cell of the beam.

The objective functions are solved by the use of the genetic algorithm (GA) method in Matlab. GA is an evolutionary algorithm inspired by the process of natural selection. The GA optimization technique has been widely used due to its ability to find out "global" optimal values for complex problems quickly. GA is also popular for the optimization of metamaterials.[51–53] The GA optimization starts with a random initial population, whose fitness values of individuals in the population are estimated based on the fitness functions. If the predefined stopping criterion is satisfied, the optimization progress ends, otherwise, offspring will be generated by virtue of biological operators such as mutation, selection, and crossover. The fitness values of the new generation will also be estimated and compared with the stopping criterion. The loop repeats until the stopping criterion is reached.

1. Single frequency range optimization case

Two single frequency optimization cases are carried out within the frequency ranges of $\boldsymbol{\Phi} = 120 \sim 160$ Hz and $\boldsymbol{\Phi} = 380 \sim 420$ Hz, respectively, which are in the proximity of the two resonance frequencies of the host beam without resonators. The parameters of the optimized resonator architectures and mass distributions for the two optimization cases are obtained as

$$\begin{gathered} q = 6, \\ [n_1, \ldots, n_q] = [1,\ 1,\ 1,\ 1,\ 2,\ 4], \\ [m_{ij}] = \begin{bmatrix} 0.0059 & 0.0072 & 0.0039 & 0.0060 & 0.0020 & 0.014 \\ & & & & 0.17 & 0.0026 \\ & & & & & 0.042 \\ & & & & & 0.043 \end{bmatrix} M_a, \end{gathered} \tag{20}$$

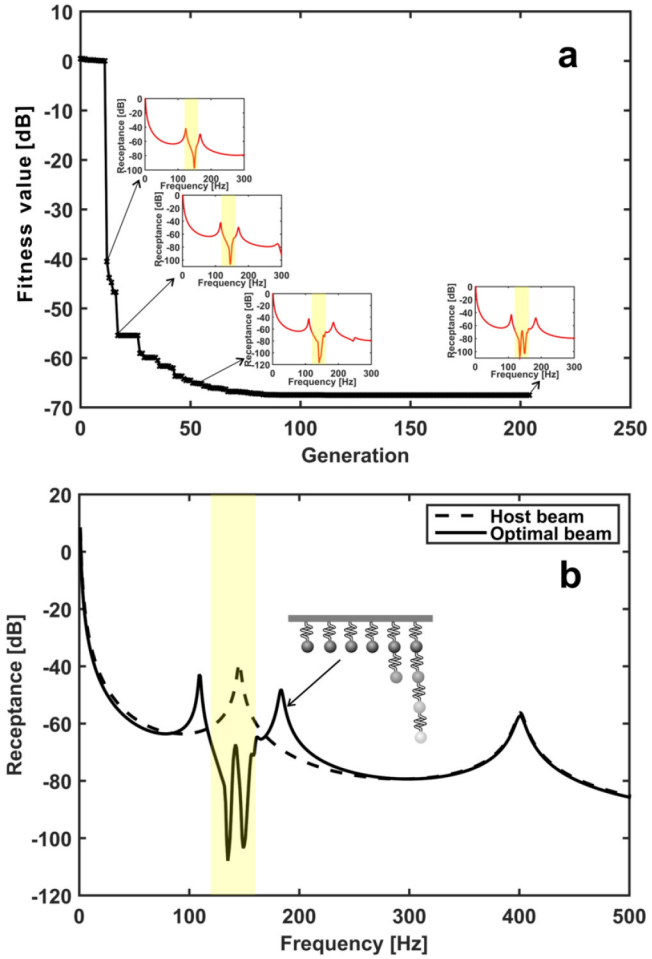

FIG. 8. The evolution of fitness values with the generation for the single frequency range optimizations in (a) $\boldsymbol{\Phi} = 120 \sim 160$ Hz, (b) $\boldsymbol{\Phi} = 380 \sim 420$ Hz. The change in receptance functions with generation are plotted in the subfigures.

$$q = 9,$$
$$[n_1, \ldots, n_q] = [1,\ 1,\ 1,\ 1,\ 1,\ 1,\ 1,\ 1,\ 2],$$
$$[m_{ij}] = \begin{bmatrix} 0.043 & 0.0018 & 0.044 & 0.039 & 0.0010 & 0.040 & 0.037 & 0.043 & 0.040 \\ & & & & & & & & 0.0035 \end{bmatrix} M_a. \tag{21}$$

The evolution of the fitness value with the generation is plotted in Figs. 8(a) and 8(b). It can be seen that the maximal receptance functions within the targeted frequency ranges decrease dramatically with the increase in the generation. Receptance functions of the bare beam and the two metamaterial beams with optimal resonator connections and mass distributions are compared in Figs. 9(a) and 9(b), respectively. The optimal resonator connection architectures are also plotted in these two figures. It can be seen from Figs. 9(a) and 9(b) that the maximal receptance functions are greatly reduced by the optimization within the targeted frequency ranges, which will result in enhanced vibration attenuation.

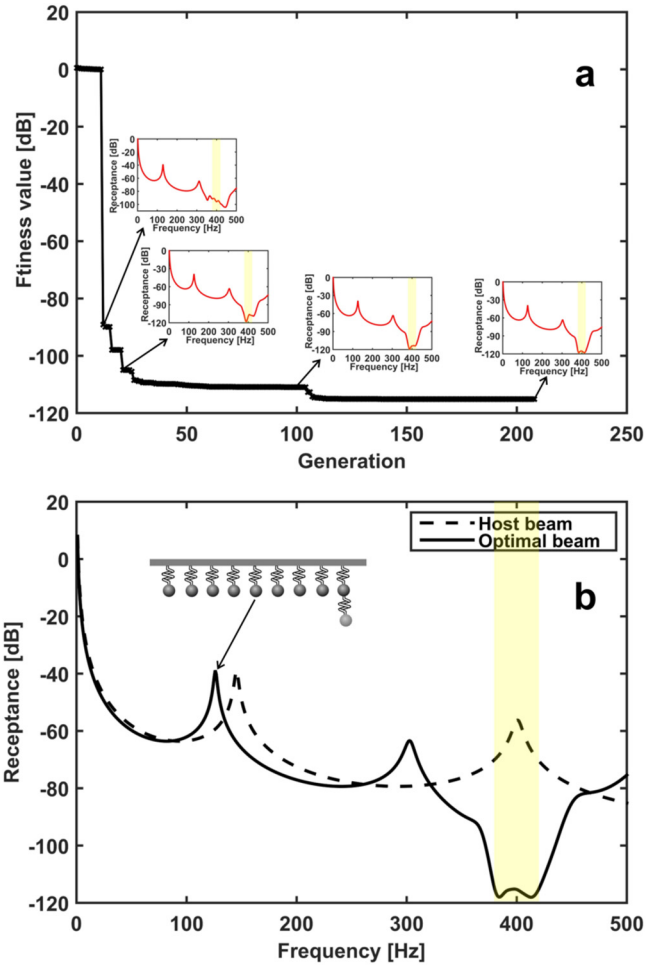

FIG. 9. Receptance comparison between the bare beam without resonators (dashed line) and the beam with optimized resonators (solid line) for the frequency range (a) $\boldsymbol{\Phi} = 120 \sim 160$ Hz, (b) $\boldsymbol{\Phi} = 380 \sim 420$ Hz. The optimized resonator connection architectures are also shown schematically in the figure.

2. Multi-frequency range optimization case

The multiple optimization case is performed in both the above-mentioned frequency ranges simultaneously, i.e., $\boldsymbol{\Phi} = 120 \sim 160$ Hz and $\boldsymbol{\Phi} = 380 \sim 420$ Hz, the weight factors are set as $\kappa_1 = \kappa_2 = 0.5$. The new optimization function is also solved by the GA method.

The optimal resonator connection methods and mass distributions are obtained as

$$q = 5,$$
$$[n_1, \ldots, n_q] = [3,\ 1,\ 1,\ 1,\ 4],$$
$$[m_{ij}] = \begin{bmatrix} 0.0066 & 0.036 & 0.039 & 0.043 & 0.052 \\ 0.010 & & & & 0.024 \\ 0.0076 & & & & 0.014 \\ & & & & 0.059 \end{bmatrix} M_a. \tag{22}$$

Figure 10 shows the change in the best fitness value of each generation during the optimization process. Figure 11 compares the receptance functions of the host beam and optimized metamaterial beam. It can be seen from both figures that maximal receptance functions within the two targeted frequency ranges are reduced simultaneously by the optimization progress, it thus can be

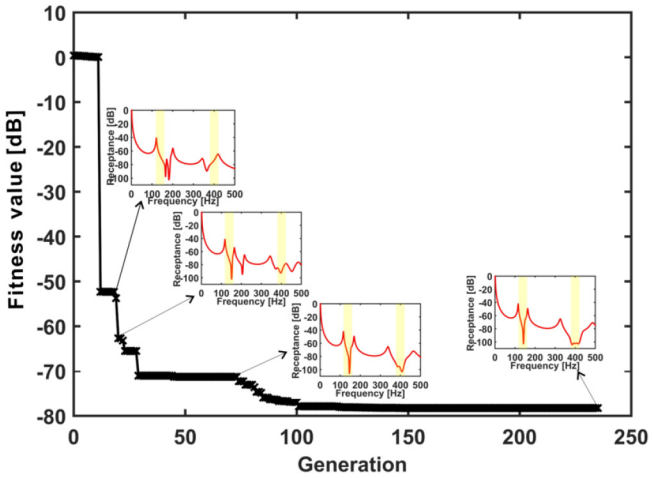

FIG. 10. The evolution of fitness values with the generation for the optimization in multiple frequency ranges $\boldsymbol{\Phi} = 120 \sim 160$ Hz and $\boldsymbol{\Phi} = 380 \sim 420$ Hz. The change of receptance functions with generation is plotted in the subfigures.

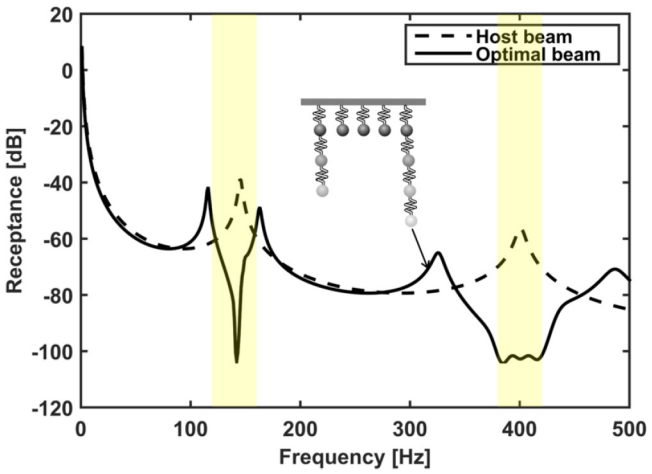

FIG. 11. Receptance comparison between the bare beam without resonators (dashed line) and the beam with optimized resonators for multiple frequency ranges $\boldsymbol{\Phi} = 120 \sim 160$ Hz and $\boldsymbol{\Phi} = 380 \sim 420$ Hz (solid line). The optimized resonator connection architecture is also shown schematically in the figure.

concluded that the proposed optimization method could lead to an effective resonator design for multi-frequency ranges.

VI. CONCLUSIONS

This paper investigated the influence of resonator connection architectures on the dynamic response of metamaterial beams with multiple resonators. An analytical model has been derived that is able to predict the vibration receptance levels for beams with multiple resonators by using the transfer matrix method. The analytical results were verified by FE models. The receptance functions of the locally resonant beams with single, in-series, and in-parallel resonators with various mass distributions were compared using the analytical model; it was shown that the connection architecture and resonant mass distribution had a great effect on the stop bands of the beams.

An optimization strategy was later developed based on the analytical model to maximize the vibration attenuation of the metamaterial beams with the resonator connection methods and mass distributions considered as design variables. The maximal receptance functions were minimized through optimization, which could lead to enhanced vibration attenuation. The optimization was conducted for both single and multiple frequency ranges. The objective function for optimization in a single frequency range could be solved by the GA method. The multi-frequency range optimization contained multiple objective functions for each individual frequency range, hence, the weighted sum method was thus adopted to build a new objective function with a Pareto optimal solution achieved. It was shown through the optimization case studies that the optimization strategy could dramatically reduce the maximal receptance function values within single or multiple frequency ranges, hence the vibration attenuation could be improved accordingly. The presented model and optimization strategy lay the first stone to develop metamaterials with enhanced stop bands with smart designed resonator connection methods and is expected to inspire future researchers to develop metamaterials with novel resonator connection architectures.

ACKNOWLEDGMENTS

We would like to acknowledge support acquired by the H2020 DiaMoND project (Grant Agreement ID No.785859), Royal Society Grant: PURSUIT, China Postdoctoral Science Foundation Grant (Grant No. 2018M643722), and the National Natural Science Foundation of China (NNSFC) (Grant Nos. 51705402 and 11904291).

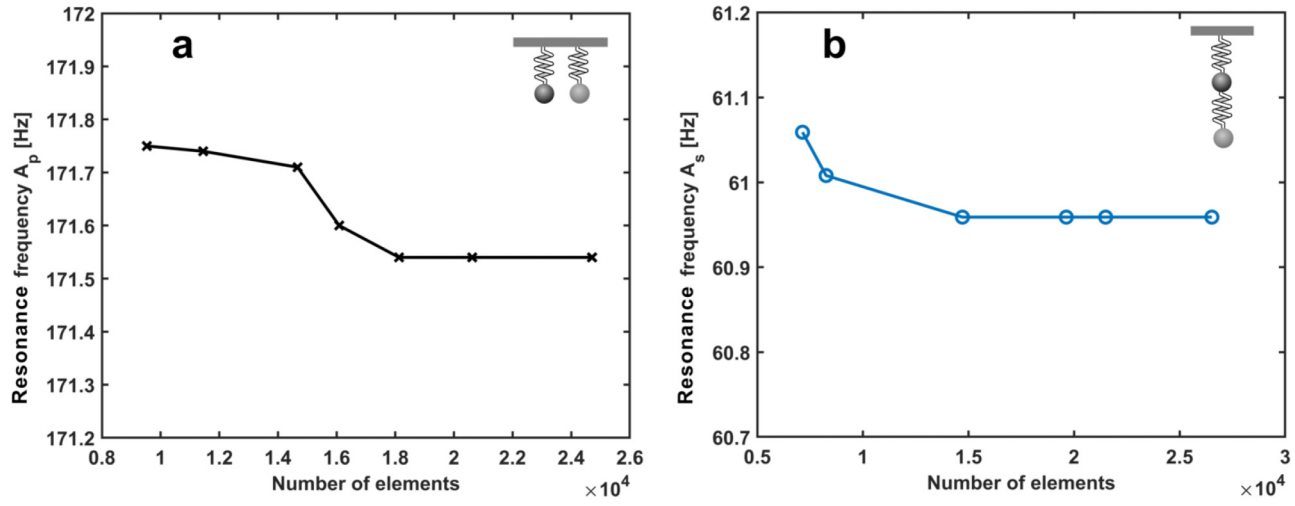

FIG. 12. Mesh convergence of FE models with respect to the resonance frequencies A_s and A_p for the metamaterial beams with (a) in-parallel and (b) in-series resonators.

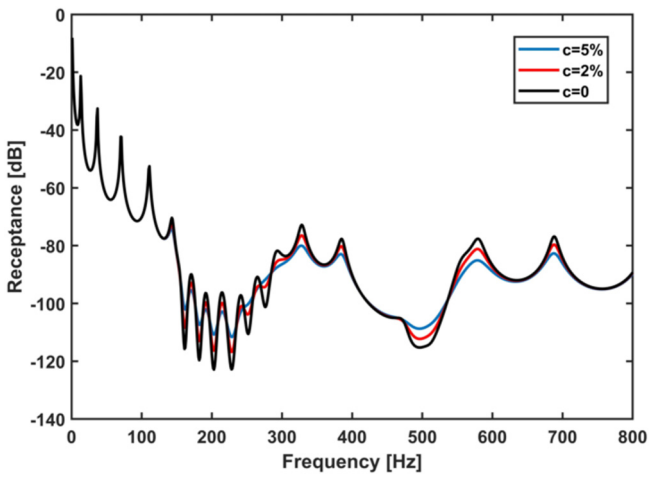

FIG. 13. Comparison of receptance function values of metamaterial beams with in-parallel resonators of different damping ratios. The geometrical and physical parameters of the beam and attached in-parallel resonators are the same as that in Sec. III.

APPENDIX A: MESH CONVERGENCE

The convergence of the FE models was verified by a mesh refinement study as shown in Figs. 12(a) and 12(b). The resonance frequencies A_s and A_p are regarded as steady and accurate when they are negligibly changed by the mesh refinement.

APPENDIX B: INFLUENCE OF SPRING DAMPING RATIO

The metamaterial beams with in-parallel resonators of the same masses and stiffnesses but different damping ratios are compared in Fig. 13. It can be seen that the damping ratio could reduce the peak and dip values on the FRF curves, i.e., flatten the curves.

DATA AVAILABILITY

The data that support the findings of this study are available within the article.

REFERENCES

[1]L. Rayleigh, "XXVI. On the remarkable phenomenon of crystalline reflexion described by Prof. Stokes," London, Edinburgh, Dublin Philos. Mag. J. Sci. **26**, 256 (1888).
[2]E. Yablonovitch, "Inhibited spontaneous emission in solid-state physics and electronics," Phys. Rev. Lett. **58**, 2059 (1987).
[3]S. John, "Strong localization of photons in certain disordered dielectric superlattices," Phys. Rev. Lett. **58**, 2486 (1987).
[4]Z. Liu, X. Zhang, Y. Mao, Y. Zhu, Z. Yang, C. T. Chan, and P. Sheng, "Locally resonant sonic materials," Science **289**, 1734 (2000).
[5]Z. Yang, J. Mei, M. Yang, N. Chan, and P. Sheng, "Membrane-type acoustic metamaterial with negative dynamic mass," Phys. Rev. Lett. **101**, 204301 (2008).
[6]T.-Y. Huang, C. Shen, and Y. Jing, "Membrane-and plate-type acoustic metamaterials," J. Acoust. Soc. Am. **139**, 3240 (2016).
[7]H. Zhang, Y. Xiao, J. Wen, D. Yu, and X. Wen, "Flexural wave band gaps in metamaterial beams with membrane-type resonators: Theory and experiment," J. Phys. D: Appl. Phys. **48**, 435305 (2015).
[8]Z. Yang, H. M. Dai, N. H. Chan, G. C. Ma, and P. Sheng, "Acoustic metamaterial panels for sound attenuation in the 50–1000 Hz regime," Appl. Phys. Lett. **96**, 041906 (2010).
[9]X. Wang, H. Zhao, X. Luo, and Z. Huang, "Membrane-constrained acoustic metamaterials for low frequency sound insulation," Appl. Phys. Lett. **108**, 041905 (2016).
[10]Y. Zhang, J. Wen, Y. Xiao, X. Wen, and J. Wang, "Theoretical investigation of the sound attenuation of membrane-type acoustic metamaterials," Phys. Lett. A **376**, 1489 (2012).
[11]N. Fang, D. Xi, J. Xu, M. Ambati, W. Srituravanich, C. Sun, and X. Zhang, "Ultrasonic metamaterials with negative modulus," Nat. Mater. **5**, 452 (2006).
[12]K. Mahesh and R. Mini, "Helmholtz resonator based metamaterials for sound manipulation," J. Phys. **1355**, 012031 (2019).
[13]C. Casarini, J. F. Windmill, and J. C. Jackson, "3D printed small-scale acoustic metamaterials based on Helmholtz resonators with tuned overtones," in *2017 IEEE Sensors* (IEEE, 2017), pp. 1–3.
[14]S. B. Gebrekidan, H.-J. Kim, and S.-J. Song, "Investigation of Helmholtz resonator-based composite acoustic metamaterial," Appl. Phys. A **125**, 65 (2019).
[15]C. R. Liu, J. H. Wu, F. Ma, X. Chen, and Z. Yang, "A thin multi-order Helmholtz metamaterial with perfect broadband acoustic absorption," Appl. Phys. Express **12**, 084002 (2019).
[16]T. Yamamoto, "Acoustic metamaterial plate embedded with Helmholtz resonators for extraordinary sound transmission loss," J. Appl. Phys. **123**, 215110 (2018).
[17]Y. Tang, S. Ren, H. Meng, F. Xin, L. Huang, T. Chen, C. Zhang, and T. J. Lu, "Hybrid acoustic metamaterial as super absorber for broadband low-frequency sound," Sci. Rep. **7**, 43340 (2017).
[18]S. K. Maurya, A. Pandey, S. Shukla, and S. Saxena, "Double negativity in 3D space coiling metamaterials," Sci. Rep. **6**, 33683 (2016).
[19]Z. Liang, T. Feng, S. Lok, F. Liu, K. B. Ng, C. H. Chan, J. Wang, S. Han, S. Lee, and J. Li, "Space-coiling metamaterials with double negativity and conical dispersion," Sci. Rep. **3**, 1614 (2013).
[20]H. Peng, P. F. Pai, and H. Deng, "Acoustic multi-stopband metamaterial plates design for broadband elastic wave absorption and vibration suppression," Int. J. Mech. Sci. **103**, 104 (2015).
[21]Z. Wang, P. Zhang, and Y. Zhang, "Locally resonant band gaps in flexural vibrations of a Timoshenko beam with periodically attached multioscillators," Math. Probl. Eng. **2013**, 146975.
[22]R. Zhu, X. Liu, G. Hu, C. Sun, and G. Huang, "A chiral elastic metamaterial beam for broadband vibration suppression," J. Sound Vib. **333**, 2759 (2014).
[23]P. F. Pai, H. Peng, and S. Jiang, "Acoustic metamaterial beams based on multi-frequency vibration absorbers," Int. J. Mech. Sci. **79**, 195 (2014).
[24]X. Xiao, Z. C. He, E. Li, and A. G. Cheng, "Design multi-stopband laminate acoustic metamaterials for structural-acoustic coupled system," Mech. Syst. Signal Process. **115**, 418 (2019).
[25]G. L. Huang and C. T. Sun, "Band gaps in a multiresonator acoustic metamaterial," J. Vib. Acoust. **132**, 031003–031006 (2010).
[26]Y. Chen, M. Barnhart, J. Chen, G. Hu, C. Sun, and G. Huang, "Dissipative elastic metamaterials for broadband wave mitigation at subwavelength scale," Compos. Struct. **136**, 358–371 (2016).
[27]Q. Q. Li, Z. C. He, E. Li, and A. G. Cheng, "Design and optimization of three-resonator locally resonant metamaterial for impact force mitigation," Smart Mater. Struct. **27**, 095015 (2018).
[28]Q. Q. Li, Z. C. He, E. Li, and A. G. Cheng, "Design of a multi-resonator metamaterial for mitigating impact force," J. Appl. Phys. **125**, 035104 (2019).
[29]Q. Q. Li, Z. C. He, E. Li, and A. G. Cheng, "Improved impact responses of a honeycomb sandwich panel structure with internal resonators," Eng. Optim. **52**, 731–752 (2019).
[30]A. T. Fabro, H. Meng, and D. Chronopoulos, "Uncertainties in the attenuation performance of a multi-frequency metastructure from additive manufacturing," Mech. Syst. Signal Process. **138**, 106557 (2020).

[31]H. Meng, D. Chronopoulos, and A. T. Fabro, "Numerical simulation data for the dynamic properties of rainbow metamaterials," Data Brief **28**, 104772 (2020).
[32]H. Meng, D. Chronopoulos, A. T. Fabro, W. Elmadih, and I. Maskery, "Rainbow metamaterials for broadband multi-frequency vibration attenuation: Numerical analysis and experimental validation," J. Sound Vib. **465**, 115005 (2020).
[33]H. Meng, D. Chronopoulos, A. T. Fabro, I. Maskery, and Y. Chen, "Optimal design of rainbow elastic metamaterials," Int. J. Mech. Sci. **165**, 105185 (2020).
[34]Z. Tong, X. Qi, and L. Li, "A method for considering a distributed spring constant for studying the flexural vibration of an Euler-beam with lightweight multistage local resonators," J. Vibroeng. **20**, 2563 (2018).
[35]E. J. P. Miranda, E. D. Nobrega, A. H. R. Ferreira, and J. M. C. Dos Santos, "Flexural wave band gaps in a multi-resonator elastic metamaterial plate using Kirchhoff-Love theory," Mech. Syst. Signal Process. **116**, 480 (2019).
[36]Y. Xiao, J. Wen, and X. Wen, "Longitudinal wave band gaps in metamaterial-based elastic rods containing multi-degree-of-freedom resonators," New J. Phys. **14**, 033042 (2012).
[37]E. Nobrega, F. Gautier, A. Pelat, and J. Dos Santos, "Vibration band gaps for elastic metamaterial rods using wave finite element method," Mech. Syst. Signal Process. **79**, 192 (2016).
[38]Z. Shuguang, N. Tianxin, W. Xudong, and F. Jialu, "Studies of band gaps in flexural vibrations of a locally resonant beam with novel multi-oscillator configuration," J. Vib. Control **23**, 1663 (2017).
[39]Y. Xiao, J. Wen, and X. Wen, "Broadband locally resonant beams containing multiple periodic arrays of attached resonators," Phys. Lett. A **376**, 1384 (2012).
[40]D. Yu, Y. Liu, H. Zhao, G. Wang, and J. Qiu, "Flexural vibration band gaps in Euler-Bernoulli beams with locally resonant structures with two degrees of freedom," Phys. Rev. B **73**, 064301 (2006).
[41]Y. Liu, D. Yu, L. Li, H. Zhao, J. Wen, and X. Wen, "Design guidelines for flexural wave attenuation of slender beams with local resonators," Phys. Lett. A **362**, 344 (2007).
[42]D. Mead, "Wave propagation in continuous periodic structures: Research contributions from Southampton, 1964–1995," J. Sound Vib. **190**, 495 (1996).
[43]L. Liu and M. I. Hussein, "Wave motion in periodic flexural beams and characterization of the transition between Bragg scattering and local resonance," J. Appl. Mech. **79**, 011003 (2012).
[44]D. Yu, Y. Liu, G. Wang, H. Zhao, and J. Qiu, "Flexural vibration band gaps in Timoshenko beams with locally resonant structures," J. Appl. Phys. **100**, 124901 (2006).
[45]M. Nouh, O. Aldraihem, and A. Baz, "Wave propagation in metamaterial plates with periodic local resonances," J. Sound Vib. **341**, 53 (2015).
[46]Y. Li, L. Zhu, and T. Chen, "Plate-type elastic metamaterials for low-frequency broadband elastic wave attenuation," Ultrasonics **73**, 34 (2017).
[47]S. Zhang, J. Hui Wu, and Z. Hu, "Low-frequency locally resonant band-gaps in phononic crystal plates with periodic spiral resonators," J. Appl. Phys. **113**, 163511 (2013).
[48]R. Zhu, G. Huang, H. Huang, and C. Sun, "Experimental and numerical study of guided wave propagation in a thin metamaterial plate," Phys. Lett. A **375**, 2863 (2011).
[49]Z. He, X. Xiao, and E. Li, "Design for structural vibration suppression in laminate acoustic metamaterials," Compos. Part B: Eng. **131**, 237 (2017).
[50]L. Sangiuliano, C. Claeys, E. Deckers, and W. Desmet, "Influence of boundary conditions on the stop band effect in finite locally resonant metamaterial beams," J. Sound Vib. **473**, 115225 (2020).
[51]H. W. Dong, S. D. Zhao, Y. S. Wang, and C. Zhang, "Topology optimization of anisotropic broadband double-negative elastic metamaterials," J. Mech. Phys. Solids **105**, 54 (2017).
[52]H. W. Dong, X. X. Su, Y. S. Wang, and C. Zhang, "Topological optimization of two-dimensional phononic crystals based on the finite element method and genetic algorithm," Struct. Multidiscip. Optim. **50**, 593 (2014).
[53]G. A. Gazonas, D. S. Weile, R. Wildman, and A. Mohan, "Genetic algorithm optimization of phononic bandgap structures," Int. J. Solids Struct. **43**, 5851 (2006).